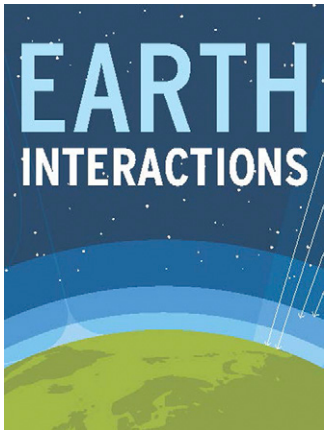

Spatiotemporal Lake Skin Summer Temperature Trends in the Northeast United States

Nathan Torbick[a]

Applied Geosolutions, Newmarket, New Hampshire

Beth Ziniti, Shuang Wu, and Ernst Linder

Department of Mathematics and Statistics, University of New Hampshire, Durham, New Hampshire

Received 6 May 2016; in final form 3 October 2016

ABSTRACT: Lakes have been suggested as an indicator of climate change; however, long-term, systematic records of lake temperature are limited. Satellite remote sensing is capable of supporting lake temperature mapping with the advantage of large-area and systematic observations. The goal of this research application was to assess spatiotemporal trends in lake skin temperature for all lakes over 8 ha across northern New England for the past three decades. Nearly 10 000 Landsat scenes for July, August, and September from 1984 to 2014 were processed using MODTRAN and MERRA parameterizations to generate atmospherically corrected lake skin temperature records. Results show, on average, lakes warmed at a rate of 0.8°C decade^{-1}, with smaller lakes warming at a faster

[a] Corresponding author address: Nathan Torbick, Applied Geosolutions, 55 Main St., Suite 125, Newmarket, NH 03857.
E-mail address: ntorbick@appliedgeosolutions.com

DOI: 10.1175/EI-D-16-0015.1

rate. Complementing regression and space–time analyses showed similar results ($R^2 = 0.63$) for lake temperature trends and found lakes, on average, are warming faster than daily maximum or minimum air temperature. No major hot spots were found as lake temperature changes were heterogeneous on a local scale and evenly distributed across the region. Maximum and minimum daily temperature, lake size, and elevation were found as significant drivers of lake temperature. This effort provides the first regionally focused and comprehensive spatiotemporal assessment of thousands ($n = 3955$) of lakes concentrated in one geographic region. The approach is scalable and adaptable to any region for assessing lake temperature trends and potential drivers.

KEYWORDS: Watersheds; Remote sensing; Statistics

1. Introduction

Lake water temperature is a fundamental driver of lake ecology and serves as a holistic measure of climate change as lake temperature represents an aggregate of lower planetary air temperature, solar radiation, phenology, and limnological forcings (Schneider and Hook 2010; Zhang et al. 2014; O'Reilly et al. 2015). Inland lakes have relatively high heat capacity, which reduces short-term variability and emphasizes longer-term variation, making lakes useful indicators of local and regional climate change. Several stressors threaten to adversely impact lake temperature and water quality, including climate change, discharge, watershed land use, and anthropogenic eutrophication (e.g., Paerl et al. 2011; Stumpf et al. 2012; Torbick et al. 2013; Torbick and Corbiere 2015). It has also been suggested that increased temperatures can enhance the frequency, duration, and intensity of cyanobacterial harmful algal blooms (CHAB) as warmer waters can create shifts in phenology, stratification, and competitive advantages (Fu et al. 2008; Moore et al. 2008, 2009; Paerl and Huisman 2008, 2009).

Many valuable long-term water temperature records exist for individual lakes that can be used to help understand spatiotemporal trends and responses to weather and climate drivers. Satellite remote sensing tools can complement traditional measures to gain a more thorough understanding of spatial variability and temperature trends given the synoptic-scale coverage over large areas. Satellite observations can be particularly useful for assessing temporal trends and spatial hot spots that cannot be observed with point samples or buoys alone. Several satellite remote sensing instruments measure thermal wavelengths, and these data can be transformed into meaningful measures of lake skin or bulk temperatures. Recent research studying 167 strategic lakes worldwide using high temporal frequency satellite imagery merged nighttime Advanced Along Track Scanning Radiometer (AATSR), AVHRR, and MODIS. This research found an average warming of 0.45°C decade^{-1}, with some lakes warming upward of 1°C decade^{-1} with noteworthy warming during the peak summer months (Schneider et al. 2009; Schneider and Hook 2010). Summer warming specifically is important in the context of climate change, water quality, and human health as water temperature can strongly influence cyanobacterial harmful algal blooms and trophic status. Summer also tends be to the time of year with peak recreational use in many regions.

Recently, the Global Lake Temperature Collaboration (GLTC) has spearheaded a coordinated approach to help understand the impacts of global and regional climate change on lakes (Lenters 2015). Some studies have indicated significant

warming of select lakes around the world with rates of warming often larger than that of the ambient air temperature. Synthesis analyses using in situ and satellite measures for 235 lakes found mean warming of 0.34°C decade^{-1} (1985–2009) and emphasized the role of climate drivers and geomorphic characteristics in driving spatiotemporal trends with summertime air temperature noted as most important (O'Reilly et al. 2015). However, not all lake temperature analyses have found warming. For example, Zhang et al. (2014) used 8-day MODIS nighttime LST (MOD11A2) and found lakes warming (0.55°C decade^{-1}) and cooling (0.53°C decade^{-1}) across the Tibetan Plateau with cooling lakes at higher elevations. Most existing lake temperature studies tend to focus on individual lakes with long-term point sampling records or large lakes with quality in situ and near-simultaneous remote sensing observations. The GLTC notes that drivers are not well understood across all lakes, and large variability exists across sampling designs, analysis methods, data quality, and continuity. It is essential therefore that global datasets of water temperature be compiled to monitor and understand long-term changes in lakes, reservoirs, and other inland water bodies (Lenters et al. 2012). These were a few reasons behind development of July–September (JAS) temperature metrics in order to robustly assess changes that also consider seasonal and interannual variability.

In the Northeast United States, only a handful of lakes have long-term temperature trend estimates. Most lakes have no long-term or systematic record and the spatiotemporal patterns are not known. The overarching goal of this study was to assess spatiotemporal lake temperature patterns in northern New England using satellite remote sensing. Two main questions are asked: Are lakes in northern New England warming, and is there a spatiotemporal pattern? To address these questions, moderate-scale, dense, time series Landsat satellite records for all lakes greater than 8 ha for July, August, and September for the past three decades were compiled. Landsat is an ideal sensor for this application, given the spatial and spectral resolutions of the platform's instruments, continuity of multiple satellites, free cost, and operational collection strategy. A complementing set of geostatistical techniques and a space–time model were employed using the Landsat satellite records along with potential climate and geomorphic drivers. This effort provides the first regionally focused and comprehensive spatiotemporal assessment of thousands of lakes concentrated in one geographic region. The approach is scalable and adaptable to any region for assessing lake temperature trends and potential drivers.

2. Lakes in the Northeast United States

Northern New England (NNE) in the United States (Maine, New Hampshire, and Vermont) is a diverse socioecological system representing a range of landscapes, lakes, and a population of nearly 3.3 million. The region covers 140 856 km^2 with dominant land types being eastern temperate forest with ecoregions of Atlantic maritime highlands, northeastern coastal zone, and Acadian plains and hills (Omernik 1987). Interior NNE has a humid continental climate (Dfb: Köppen climate classification) with cold winters and seasonal patterns. Elevation ranges from sea level along the coast to 1926 m in interior mountains stretching throughout the western portion of NNE. Lakes often serve as residential and recreational attractions with land-use patterns reflecting lake features (Torbick and Corbiere 2015). Most lakes are classified as being in "good" condition based on a suite of

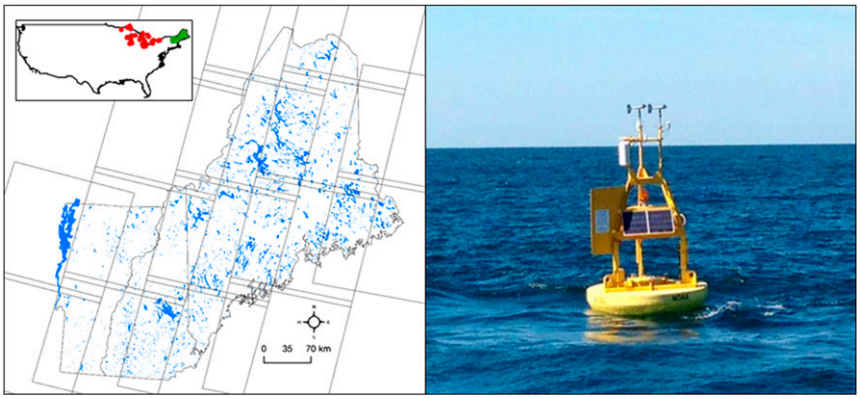

Figure 1. (left) Northern New England study area with lakes (blue), locations of calibration buoys (red), Landsat path row footprints, and (right) example NOAA buoy.

assessment parameters (e.g., chlorophyll-*a*, Secchi depth, plankton, total phosphorus, taxa, and lake shore habitat) with half of all lakes falling within the mesotrophic category (Torbick et al. 2014). Several valuable lake monitoring databases collected by volunteer groups and citizen scientists provide some of the best records for lakes. In the Northeast, typically no more than 15% of a state's lakes are sampled using traditional field measurements in a given year. For instance, Maine has over 6000 water bodies categorized as significant, yet rarely are more than 400 lakes sampled in a given year; New Hampshire typically samples about 150 of 950 lakes. A handful of federally funded and state agency programs operate buoys on select lakes; however, these data are also limited in their spatial and temporal coverage. This study considered 3955 lakes after removing lakes <8 ha and/or lakes too narrow for pure pixels (Figure 1).

3. Methods

3.1. Generating Landsat temperature records

Spatially comprehensive or ''wall-to-wall'' maps of lake skin temperature over a large geographic region like NNE requires the use of moderate resolution (<30 m) sensors, such as Landsat, because of the spatial configuration of small- to medium-sized lakes and ponds. Landsat provides the longest and only seamless record of surface temperature at the moderate spatial scales required to monitor human activities (Schott et al. 2012). Landsat 5 launched into orbit in 1984 equipped with the Thematic Mapper (TM) instrument capable of observing thermal infrared wavelengths at a spatial resolution (pixel size) of 120 m. Landsat 5 TM has a 16-day repeat overpass for the same geographical footprint. Landsat 7 Enhanced Thematic Mapper Plus (ETM+) launched into orbit in 1999 with instruments capable of observing thermal wavelengths at a spatial resolution of 60 m. Landsat 7 ETM+ has the same repeat frequency as Landsat 5 TM, although offset by 8 days. Together these two sensors provided an image every 8 days when both satellites were

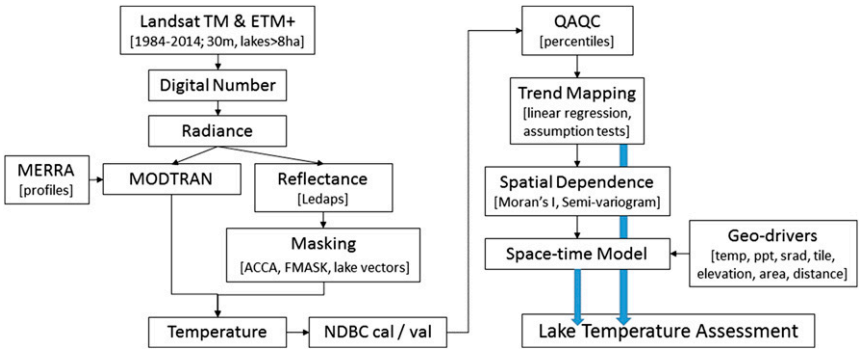

Figure 2. Conceptual workflow to derive Landsat lake temperature and assess for spatiotemporal patterns.

collecting data (e.g., 1999–2012); otherwise, the repeat frequency is once every 16 days (e.g., 1984–99). The thermal infrared channels of TM and ETM+ cover the 10.4–12.5-μm portion of the electromagnetic spectrum with two 8-bit gain settings. All Landsat satellites follow a sun-synchronous orbit with a footprint of approximately 180 km $\times$ 180 km, and 12 scenes were required for wall-to-wall mapping of NNE. Adjacent Landsat paths have some overlap, resulting in some lakes having more observations and an uneven sampling frequency for any given combinations of lakes. All Landsat data were obtained from USGS Earth Explorer (http://earthexplorer.usgs.gov/), which serves the open access archives.

All Landsat 5 TM and Landsat 7 ETM+ for July, August, and September were obtained over NNE. As noted, the JAS time window has been identified as a meaningful and robust measure that considers seasonal and interannual variability. Imagery was obtained with standard radiometric and geometric terrain corrections applied using the best available ground control points and digital elevation models. The entire archive of Landsat 4, 5, and 7 recently underwent thermal infrared radiometric calibration to increase the utility of the measurements for studying ecosystems (Schott et al. 2012). In 2003, the Landsat 7 scan line corrector (SLC) malfunctioned causing no data stripes in about 40% of the Landsat 7 scenes. The SLC off pixels were treated as no data using SLC masks. To generate cloud masks, Landsat data were preprocessed using a work flow mirroring the Landsat Ecosystem Disturbance Adaptive Processing System (LEDAPS) protocol developed at NASA (e.g., Masek 2006; Irish et al. 2006). The Automated Cloud Classification Algorithm (ACCA) and the Function of MASK (Fmask) were both used to mask potential cloud and shadow pixels.

It is not uncommon to see the use of apparent or at-sensor brightness for assessing landscape temperature; however, this leaves potential sources of error from the atmosphere in the processing chain. Therefore, to generate water skin temperature using Landsat, we followed the lineage of previous studies for generating calibrated lake skin temperature. In this study, Landsat measurements were transformed from digital number to radiance to temperature (Figure 2). A nominal fixed emissivity value for water (0.95) was applied. Temperature was calculated using atmospherically corrected radiance using the inverse Planck function to

convert from inband radiance to Celsius degrees. We relied on the moderate resolution atmospheric transmission (MODTRAN) radiative transfer model (version 5.3) parameterized with custom atmospheric profiles (vertical profile) retrieved from the Modern-Era Retrospective Analysis for Research and Applications (MERRA) data using the Open-Source Project for a Network Data Access Protocol (OPeNDAP). The atmospheric profiles included absorbing gas, H_2O, and ozone mixing ratios for approximately 60 pressure layers.

Thorough sensitivity testing for parameterization was performed to validate the preprocessing flow using NOAA in situ measurements in the Great Lakes available from the National Data Buoy Center (NDBC). No buoys (collocated and temporally aligned with Landsat measurements) in NNE provided enough robust data to perform calibration and validation, so the best available (e.g., Great Lakes) were used following the lineage of previous work (e.g., Schneider and Hook 2010). Long-term (>30 years) buoy observations (45001, 45002, 45003, 45004, 45005, 45006, 45007, and 45008) across each Great Lake were obtained for JAS 1984–2014. NDBC collects measurements at least once an hour and near-simultaneous observations between the corresponding Landsat satellite overpasses and buoy measurements were extracted. These data were also used to test for potential differences between TM and ETM+ and temporal degradation.

Lake vectors from the USGS National Hydrography Dataset were used to extract the Landsat thermal measurements. Lake vectors were examined against high-resolution imagery [National Agricultural Imagery Program (NAIP)] to ensure quality. Vectors were buffered inward by one pixel to avoid potential noise from mixed pixels and land features. Average Landsat temperature values masked for clouds, shadows, islands, and SLC gaps were then generated for each observation. As a result, the total number of observations for a lake will vary by year and by location due to the path row footprint, clouds, and potential down time for the satellite.

3.2. Geodrivers

A strategic set of landscape and meteorological drivers (geodrivers) was tested as potentially influencing lake skin temperature patterns and trends. A general hypothesis was that climate change or increasing air temperatures are driving lake temperatures higher. Other factors, such as landscape location, elevation, and lake size, have been suggested as influencing hot spots and trends. In this study we considered minimum, mean, and maximum temperatures; solar radiation; and precipitation at each lake from Daymet. Daymet provides 1-km gridded estimates of daily weather parameters for North America for 1980 through the latest full calendar year. Daymet is supported by funding from NASA through the Earth Science Data and Information System (ESDIS) and the Terrestrial Ecosystem Program and the U.S. Department of Energy's Office of Science. The ground-based meteorological station data required for running Daymet data have been acquired through the National Climatic Data Center, the National Resource Conservation Service, and additional datasets obtained through the generosity of the Mexican and Canadian governments. The data are served by Oak Ridge National Laboratory (ORNL) Distributed Active Archive Center (DAAC). At each lake the mean for the given meteorological driver, that is, minimum temperature, were generated using the daily Daymet values. Elevation of each lake was obtained from a digital

Table 1. Geodrivers considered as influencing spatiotemporal lake skin temperature patterns.

GeoDriver	Spatial	Temporal	Source
Temperature minimum (tmin)	1 km	Daily	Daymet
Temperature maximum (tmax)	1 km	Daily	Daymet
Solar radiation (srad)	1 km	Daily	Daymet
Precipitation (prcp)	1 km	Daily	Daymet
Elevation	30 m	—	SRTM
Lake surface area	Vector	—	Spatial analyses
Distance to ocean (D2O)	m	—	Spatial analyses
Path row (sampling frame)	Vector	—	USGS

elevation model to gauge any potential variability across height gradients. Surface area and the distance to the ocean were calculated for each lake within GIS. Finally, the path row (tile) for each Landsat scene was used as a variable to test if sampling frequency (or path row) influenced the spatiotemporal trend assessment (Table 1).

3.3. Quality assurance quality control

Because of potential noise (clouds and atmospheric attenuation that was not treated) within operational preprocessing of thousands of Landsat scenes, diligent treatment for outliers was carried out. Ultimately, a filtering routine was chosen that first grouped lake observations by size and uses the 25th percentile (Q1), 75th percentile (Q3), and interquartile range (IQR) to calculate a lower bound = Q1–1.5 × IQR and an upper bound = Q3 + 1.5I × IQR for each group. Then observations from each group below the group's lower bound or above the group's upper bound were removed. Sampling frequency, day of year, and number of observations were all thoroughly tested as cofounding factors and sources of uncertainty. Last, for a limited number of cases we compared available satellite observations against ground truth (364 of the 384 393 total satellite observations) where collocated and simultaneous (same day) in situ temperature and satellite temperatures existed.

3.4. Exploratory trend mapping

The first step carried out to assess trends in lake skin temperature fits a regression model to the satellite-derived temperature observations for each of the 3955 lakes separately. Fitting separate models for each lake instilled the assumption that lakes were independent of each other. A day of year (DOY) quadratic adjustment factor was integrated to treat intra-annual variability that may have been confounded with sampling frequency across lakes and tiles:

$$\begin{aligned}\text{Temp C} = {} & \beta_0 + \beta_{\text{year}}[\text{Year} - \text{mean(year)}] + \beta_{\text{DOY}}[\text{DOY} - \text{mean(DOY)}] \\ & + \beta_{\text{DOY}^2}[\text{DOY} - \text{mean(DOY)}]^2 + \varepsilon.\end{aligned}$$

The estimate for β_{year} (trend estimate) was of particular interest since it represents the average temperature change in degrees Celsius per year. A lower and upper 95% confidence estimate for the trend of each lake was calculated to quantify

trend uncertainty. Confidence estimates were based on large sample theory asymptotics:

$$\beta_{\text{year}} \pm \text{se}_{\text{trend}} \times qt(0.975, \quad df = \text{lake obs} - 4).$$

Individual lake regression models were further investigated for model assumption violations using a global test proposed by Peña and Slate (2006) that has been implemented in the R package glvma available on the Comprehensive R Archive Network (CRAN). Peña and Slate's (2006) global linear assumption test simultaneously tests all four of the linear model assumptions, which are linearity, homoscedasticity, uncorrelatedness, and normality. Large values of the global statistic indicate at least one of the assumptions may have been violated. The global statistic is a sum of four component statistics that can be investigated further to determine specific violations. For example, large values of the first component suggest the residuals are skewed.

Peña and Slate (2006) also suggest a method for detecting outliers and influential points using a leave-one-out deletion statistic that was used as a second iteration of outlier removal. To use this approach, the global statistic was recalculated the same number of times as the number of observations in each model, each time excluding one observation. Then if one observation was an outlier or influential point, when it was removed the global statistic had a different p value. To make this determination, plotting the p values versus the observation number was suggested. Since plotting was not feasible for many models, a conservative rule was used for single lake modeling; observations that had p values more than three standard deviations different from the mean p value for all observations were removed.

3.5. Assessing spatial relationships

Exploratory spatial statistics were applied to assess for spatial dependence among lake temperature trends that were estimated via least squares. When spatial dependence was present, an analysis that explicitly models this dependence will have more power determining the statistical significance of trend estimations than individual lake analyses. Furthermore, an analysis that incorporates the spatial dependence will smooth individually estimated extreme trends in cases where individual trends were based on small sample sizes, and it enables the statistical assessment of spatial patterns such as hot spots.

Moran's I statistic was used to test whether the lake trends exhibit statistically significant spatial dependence and require the consideration of more spatially aware analyses. In this case, Moran's I statistic calculates the ratio between a lake trend outcome and its spatial neighbors, which were determined using a Delaunay triangulation of the geocoded lake centroids and spatial weights. The null hypothesis of the Moran's I test states that the spatial processes promoting the observed pattern of values was due to random chance; in another words, there was no spatial autocorrelation. When the test results in a large p value, it was possible that the spatial trend was due to randomness. If the test resulted in a small p value and the test statistic was positive, the observations in the dataset were more spatially clustered than would be expected if the underlying spatial processes were random. See Moran's I below:

$$I = \frac{n}{S_0} \frac{\sum_{i=1}^{n} \sum_{j=1}^{n} w_{i,j} z_i z_j}{\sum_{i=1}^{n} z_i^2},$$

where z_i is the deviation of a trend for a given location from its mean, $(x_i - X)$, $w_{i,j}$ is the spatial weight between locations i and j, n is the number of locations, and S_0 is the aggregate of all the spatial weights $S_0 = \sum_{i=1}^{n} \sum_{j=1}^{n} w_{i,j}$.

The Z_I – score for the statistic was computed as

$$Z_I = \frac{I - E[I]}{\sqrt{V[I]}},$$

where

$$E[I] = -1/(n-1),$$

$$V[I] = E[I^2] - E[I]^2.$$

In the presence of significant spatial autocorrelation, the empirical semivariogram, which summarizes variance over increasing separation distances (Bailey and Gatrell 1995), can be used as a tool to understand the maximum distance at which lake trends still exhibit spatial correlation. The semivariogram function $\gamma(h)$ was originally defined by Matheron (1963) as half the average squared difference between points separated by a distance h:

$$\gamma(h) = \frac{1}{2|N(h)|} \sum_{N(h)} (Z_i - Z_j)^2,$$

where $N(h)$ is the set of all pairwise Euclidean distances $i - j = h$, $|N(h)|$ is the number of distinct pairs in $N(h)$, and Z_i and Z_j are data values at spatial locations i and j. Distances for lake trends were calculated based on the geocoded lake centroids.

3.6. Space–time model

A space–time model was used to treat potential spatial dependence within the data as well as assess potential drivers of lake skin temperature. Space–time models can be used when data are collected and potentially related across time and space. Assessments based on space–time data need to take into account the spatial dependence between nearby locations and the temporal dependence of observations at locations. The main advantage of a space–time model over separate time series analyses is that in situations where individual time series have few data points, a space–time model that simultaneously uses all data and incorporates the spatial dependence typically provides more robust trend estimation. There are many space–time models that can be used, but most can be described as either a dynamical model (i.e., a spatial field that changes in time) or a descriptive model, such as a set of spatial varying time coefficients (Cressie and Wikle 2011).

In this study, the different sampling frequency—either from path row, clouds, or different sensors—created an uneven frequency across space and time, which implies the second type of model (descriptive) was more appropriate. Furthermore, this approach allowed the comparison of spatially varying time coefficients with the trend coefficients estimated individually for each lake during the exploratory analyses. A space–time model developed by Lindström et al. (2014) was applied in this study because of the ability to treat unique sampling frequency issues. In this model, spatiotemporal variability of space–time data was modeled through the use of spatially varying temporal basis functions. A key component of this model was the robust and flexible method used to deal with potentially inconsistent space–time observations (i.e., not all locations were measured at all the time points).

The model was fit using the package SpatioTemporal, available in R, which provides maximum likelihood estimates of model parameters based on a profile likelihood and restricted maximum likelihood algorithm that improves computational efficiency (Lindström et al. 2013). Lindström et al. (2014) show that computational costs of their implementation grow less than $O(N^3)$, where N was the total number of observations at all locations. However, the dominating computational element for their implementation will still grow on a scale of $O(m^3n^3)$, where m is the number of basis function and n was the number of spatial locations. For this reason, a robust and representative subset of lakes ($n = 1359$) across NNE was utilized. Lakes for the subset were chosen so that the same geographic region and feature distributions (i.e., size, elevation, distance to ocean, and sampling frequency) were integrated.

Lindström et al.'s (2014) space–time model has the form

$$y(s, t) = \mu(s, t) + \upsilon(s, t),$$

where $y(s, t)$ denotes the satellite-derived lake skin temperatures indexed by lake location s and year t, $\mu(s, t)$ is the mean field for the water temperatures with both spatial and temporal correlations, and $\upsilon(s, t)$ is the space–time residual Gaussian field with zero mean and spatial dependence variance. The observations were assumed independent in time.

The mean field has the form

$$\mu(s, t) = \sum_{l=1}^{\mathrm{L}} \gamma_l M_l(s, t) + \sum_{i=1}^{m} \beta_i(s) f_i(t),$$

where $M_l(s, t)$ are the drivers that vary over space and time, γ_l is the coefficient effect of each space–time driver, $\{f_i(t)\}_{i=1}^{m}$ is a set of smooth basis functions used to track the time trend of the water temperatures, and $\beta_i(s)$ are spatially varying coefficients for the temporal trends.

The spatially varying coefficients of the basis functions β_i were modeled using universal kriging:

$$\beta_i(s) \in N[X_i\alpha_i, \Sigma_{\beta_i}(\theta_i)],$$

where the mean in the kriging is constructed as a linear regression on drivers that only vary over space. The effect of the spatial covariates on the spatially varying

basis function coefficients was the term α_i. The spatial dependence of the spatially varying coefficients is modeled in a set of variance–covariance matrices denoted by $\Sigma_{\beta_i}(\theta_i)$. These covariance matrices have a form defined by the exponential covariance function that is based on distances between lake centroids. Spatially varying basis function coefficients were assumed to be independent of each other.

Last, the space–time model was assessed for fit using the root-mean-square error (RSME) and R^2. RSME and R^2 were calculated for the mean field $\mu(s, t)$ and the full model. The mean field is the main model with spatial and temporal correlations but no residual field included, while the full model is the mean field together with the residual field.

3.7. Limitations

We note limitations exist within the data and our analyses. We focused on summer temperatures and trends while others have considered additional variables such as winter temperatures, ice cover, and depth (Weyhenmeyer et al. 2004; O'Reilly et al. 2015). For example, recent work by Zhong et al. (2016) shows meteorological forcing from antecedent winter and spring is likely an important driver for the temperature patterns of the Great Lakes. The remote sensing observations were limited to the skin or water surface temperature. The remote sensing measures might not be representative of deep depths, stratified lakes, or diurnal variability. The midmorning local overpass time of the collection might not be representative of nighttime or maximum temperatures in a given lake. The major challenge in this statistical model for this application was that it becomes computationally intensive to estimate the parameters for a large number of locations. Therefore, we recommend ample computational resources if executing this approach over large regions.

4. Results and discussion

4.1. Landsat thermal calibration accuracy

To tune the thermal processing routine for tens of thousands of Landsat images, a robust and automated approach was executed. The automated processing of Landsat temperature showed relatively robust outcomes ($R^2 = 0.86$) with no bias between sensors (TM vs ETM+) or drift over time (1984–2014). The outcomes were sensitive to a wide range of values (2°–27°C) and across the buoys in all the Great Lakes (Figure 3). The approach tended to slightly overestimate skin temperature; however, this was also consistent across factors (i.e., lake, buoys, sensors, and time). Cloud masking relied upon applying both ACCA and Fmask, as each approach had certain conditions in which it performed well and had limitations. Case study analyses showed that light haze conditions on occasion were not masked by either ACCA or Fmask and resulted in low values. This was where the additional quality assurance/quality control (QAQC) was effectively used to filter outlier observations. Case study investigations showed most of these outliers were from atmospheric conditions not masked using automated cloud identification techniques. Alternative filtering techniques (i.e., thresholding-based buoy observations) were considered, but ultimately the automated procedures based on the

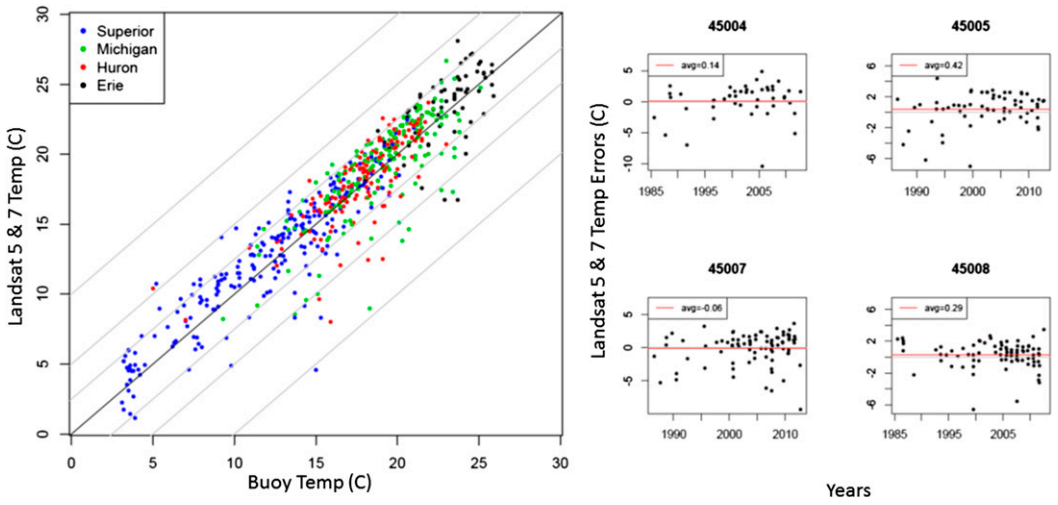

Figure 3. (left) Scatterplot showing operational Landsat temperature observations compared against simultaneous NOAA buoy temperatures color coded by lake and (right) example residual errors for four selected buoys showing average error −0.06° to 0.42°C.

distribution of the data were robust and based on a spatially aware statistical approach that considered the local conditions.

4.2. Exploratory trend mapping of NNE lake skin temperature

The exploratory lake skin temperature trends estimated via least squares regression (see section 3.4) showed that most lakes in this region have warmed with an average increase of 0.8°C decade^{-1} (Figure 4). This average increase in NNE was higher than the mean rate of increased warming identified by previous work using 235 large lakes dispersed around the globe (O'Reilly et al. 2015). The trend estimates range from −2° to just under 3°C decade^{-1}. We note that this research focused on thousands of lakes with the majority being small (<1 km^2). The spatial distribution of these trends was heterogeneous on a local scale with no major hot spots or clusters throughout the region on a broad scale. A few regions, such as northwestern and easternmost Maine, had fewer observations during the target temporal window that gave the appearance of unique regions. However, the values in these two regions violate assumptions and do not have significant trends. These locations had large temporal gaps in the Landsat coverage due to clouds. Most regions have a lower uncertainty estimate slightly larger than 0 and an upper uncertainty estimate near 1°C increase per decade.

Some caution should be taken when considering extreme trends even when they have significant p values. Figure 5 illustrates a case study of two lakes with extreme trends: one decreasing and the other increasing. Both of these extreme cases have fewer observations overall (around 30) and were sparsely sampled during stretches in the 1980s and 1990s. Figure 5 illustrates outliers that were removed using the percentile rule (red boxes) and the deletion statistic (green triangle). In the case of

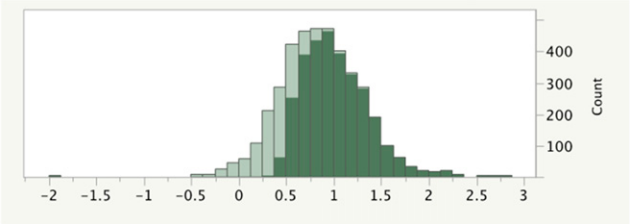

Figure 4. Histogram of exploratory lake skin temperature trend estimates in °C decade^{-1}, where dark green indicates trends with a *p* value less than 0.05.

the decreasing trend (left plot), if the one outlier removed using the deletion statistic had not been removed, the trend would be less extreme and have a p value larger than 0.05. The trend estimated in the space–time model was also less extreme (blue line). The spatially aware smoothing of extreme trends in the cases of small sample sizes was another advantage of a space–time model that incorporates spatial autocorrelation.

The exploratory lake trend regression models had a range of goodness-of-fit values. The R^2 values ranged from about 0.1 to 0.9. Over 2000 of the models have been flagged for having possible linear model violations, and these models also correspond to most of the low R^2 values. Further investigations of the components of the test statistics show that most of the violations were likely related to the error distributions being skewed and deviating from the normal distribution's kurtosis (Figure 6).

The outlier removal process showed some sensitivity to these distributions and diligent treatments were considered. One example where the outlier removal

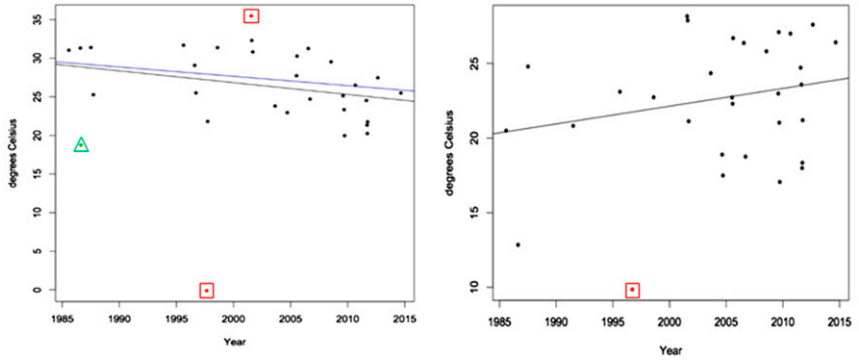

Figure 5. Examples of outliers and extremes due to few observations and wide variability in derived thermal records. Red boxes and green triangles indicate observations excluded from further analysis using the percentile removal filtering and Peña and Slate (2006) test statistics, respectively. Black lines indicate trends estimated using regression and, in the left plot only, the trend estimated in the space–time model is shown in blue.

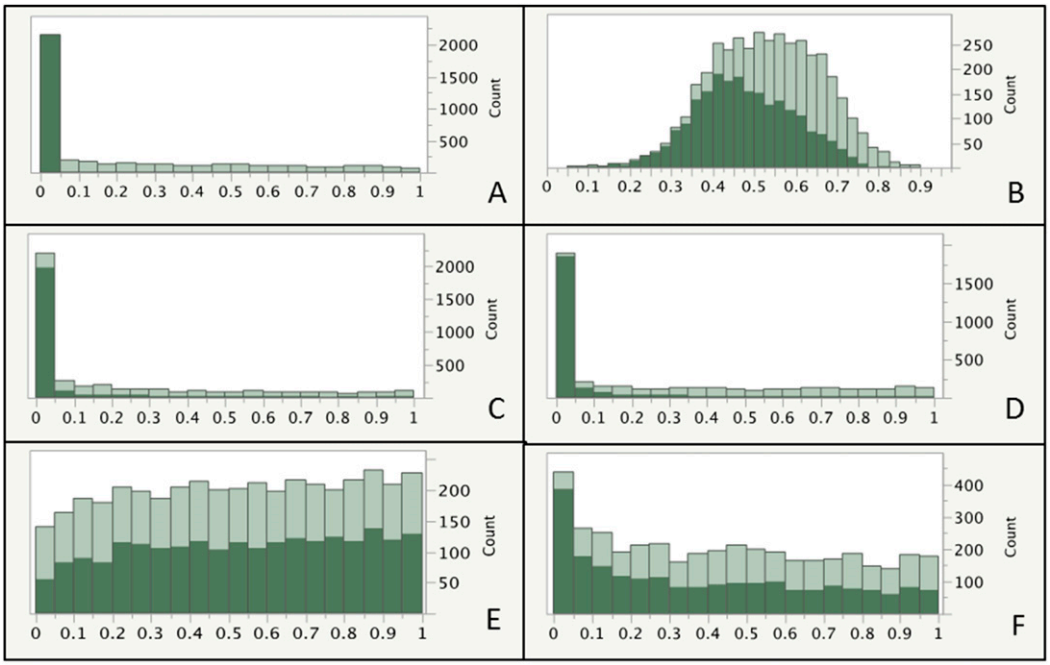

Figure 6. Left: Histograms for (a) *p* and (b) R^2 values for the global test statistic and (c) skewness, (d) kurtosis, (e) misspecified link function, and (f) heteroscedasticy.

procedure did not seem sensitive enough was Lake Winnipesaukee (Figure 7). This is the largest lake in New Hampshire and was the lake with the most satellite observations. The plots show outliers removed by percentile (red) and by the test statistic (green). The Peña and Slate (2006) approach removes two observations of temperatures around 15°C, but there were a number of other observations around 15°C in mid- to late July that should have likely been removed as well. In contrast, the outlier method was sufficient for China Lake in Maine. The R^2 value was fairly high at 0.73, and the test statistic did not flag any linear model assumptions. The plot also shows that in situ surface measurements have a very large variability relative to the satellite measurements as this was one lake with same-day independent ground truth and satellite temperature records. This case study lake shows the approach to map lake temperature performed well.

The geostatistical assessment for spatial dependence showed that spatial autocorrelation existed in the trend outcomes and lake data. Moran's I statistic (0.059 55; *p* value: 0.000 139) showed the observations were more clustered than would be expected by random chance, and the semivariogram showed (nugget: 0.001; sill: 0.003; range: 111.12 km) that lakes located within 112 km had some spatial autocorrelation. This was not surprising given the geography and characteristics of lakes in NNE being interrelated across space and time. The spatial dependency tests indicated that explicitly modeling the spatial correlation should be considered to provide more robust, or complementing, analysis of lake skin temperatures across NNE at these scales.

Winnipesaukee (km^2)	184.757	
Number of observations	246	
Average temp (°C)	22.26	
Year trend (° C / decade)	0.46	
p-value trend	0.018	
R-square	0.21	
Global test p-value	0	
p-value for components of global test	1. Skewness	0
	2. Kurtosis	0
	3. Link function	0.78
	4. Heteroscedasticity	0.82
China Lake (km^2)	15.952	
Number of observations	119	
Average temp (°C)	24.39	
Year trend (° C / decade)	0.7	
p-value trend	<0.001	
R-square	0.73	
Global test p-value	0.88	
p-value for components of global test	1. Skewness	0.53
	2. Kurtosis	0.90
	3. Link function	0.42
	4. Heteroscedasticity	0.70

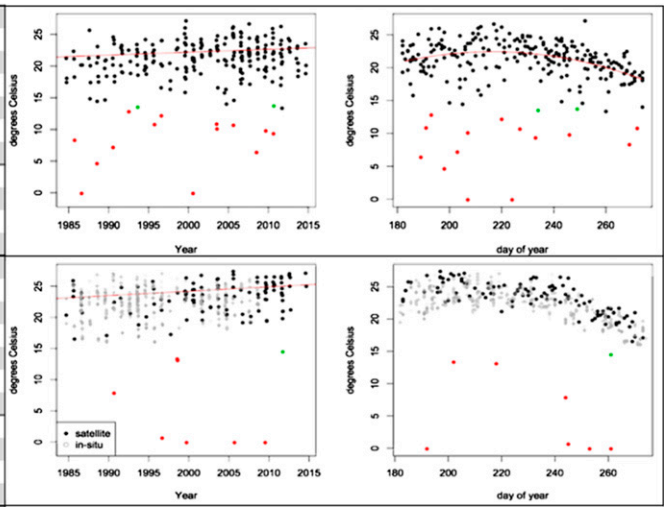

Figure 7. Summary regression and violation statistics for Lakes Winnipesaukee (New Hampshire), the largest lake (184 km^2) with the most satellite observations (246), and China Lake (Maine) as example case studies. Here, the initial removal process was not sensitive enough for Lakes Winnipesaukee as the green circles show observations not removed. While for China Lake the filtering approach worked well with a moderately high R^2 (0.73) and no violations of linear model assumptions. The gray dots for China Lake illustrate in situ, and large variability is evident in the ground truth observations.

4.3. Space–time model

The space–time model was used to treat spatial dependence and help assess drivers of lake skin temperature in northern New England. Below are three example prediction plots for case study lakes highlighting strong model performance (Figure 8). Examples shown include Spring Lake in New Portland, Maine (12611); Thorndike Pond in Jaffrey, New Hampshire (4425263); and Converse Meadow Pond in Rindge, New Hampshire (6234554). Plots show the observed Landsat TM and ETM+ temperature values (red line) and the space–time predictions (black line) based on the parameterized model with 95% confidence intervals (gray). In general, the model was robust across lake types (size, location, elevation, and trophic status) with magnitude and amplitude of trends well captured and within uncertainty bounds for the majority of observations. As expected, the space–time model tended to be smoother with fewer extremes values.

The model parameters were fit with maximum likelihood estimation summarized in Table 2. A feature of the space–time model was the identification and, ultimately, ranking of the geodrivers in relation to the lake skin trends. Accordingly, the drivers that most strongly correlated with lake skin temperature were daily maximum and minimum air temperature. This top ranking, using a regionally comprehensive and diverse set of lakes, was similar to recent finds of O'Reilly

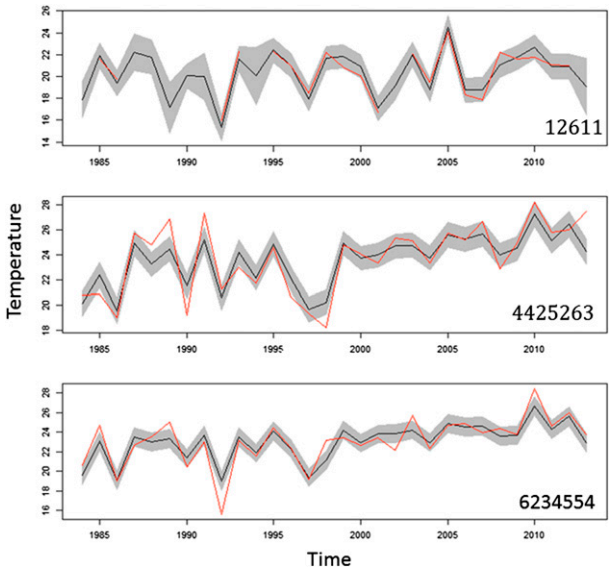

Figure 8. Space–time model outcomes (black), Landsat observations (red) using pointwise interpolation, and 95% confidence bands (gray shading) for three example lakes (Spring Lake, Thorndike Pond, and Converse Meadow Pond) showing strong correspondence over time and the ability of the model to capture dynamic range and variability.

et al. (2015). The coefficients for both of these drivers were positive, which indicated the higher the air temperature, the higher the lake skin temperature. In particular, a 1°C increase in the daily maximum air temperature resulted in a lake skin temperature increasing by 0.43°C on average. A 1°C increase in the daily minimum air temperature resulted in lake skin temperature increases of 0.28°C on average. These outcomes showed maximum air temperature resulted in more warming compared to minimum air temperature.

In the Northeast, average maximum and minimum temperatures are predicted to increase, on average, by 2.3°C over the next half century (Hayhoe et al. 2007, 2008; Wake et al. 2014). This research suggests lakes will continue to warm as rates of air and lake temperatures have cotrended upward. More mild winters have been suggested to contribute to earlier stratification, less ice, and greater solar radiation amplifying subsequent warming due to higher heat absorption (Zhong et al. 2016). In the Northeast, warming lakes have substantial societal implications as higher lake temperatures have been noted as a driver of cyanobacterial harmful algal blooms (Paerl and Otten 2013), which have been associated with public health risks (Torbick et al. 2014).

Log-transformed lake surface area had a significant negative influence on trends. This research showed that, for lakes in NNE, more lake surface area resulted in less rapid warming compared to smaller lakes. Small ($<1\,\text{km}^2$; $n = 778$), medium (1–5 km^2; $n = 430$), and large (5+ km^2; $n = 151$) lakes had a mean trend of 1.05°, 0.86°, and 0.70°C decade^{-1}, respectively, and were statistically different. This research shows that smaller lakes and ponds were more susceptible to change

Table 2. Parameter estimate from spatiotemporal model.

Model section	Coefficient	Parameter	Std dev	*t* stat	*p* value
Space–time drivers (gamma)	Tmax	0.432	0.040	10.699	0.000 00
	Tmin	0.281	0.050	5.667	0.000 00
	Srad	0.005	0.004	1.264	0.179 36
	Prcp	0.068	0.043	1.591	0.112 47
Constant basis function drivers (alpha_f0)	Intercept	7.926	1.970	4.023	0.000 12
	PATH	−0.135	0.094	−1.436	0.142 26
Trend basis function drivers (alpha_f1)	Intercept	0.547	0.177	3.085	0.003 42
	log.Elev	−0.053	0.020	−2.711	0.010 10
	log.AREASQKM	−0.070	0.006	−11.672	0.000 00
Constant basis function spatial correlation	log.range.const.exp	−0.716	0.386	−1.856	0.071 29
	log.sill.const.exp	−0.884	0.044	−19.888	0.000 00
Trend basis function spatial correlation	log.range.V1.exp	−0.428	1.696	−0.252	0.386 45
	log.sill.V1.exp	−3.737	0.123	−30.472	0.000 00
Space–time error field	nu.log.range.exp	5.044	0.079	64.198	0.000 00
	nu.log.sill.exp	1.385	0.070	19.735	0.000 00
	nu.log.nugget.(Intercept).exp	−0.067	0.012	−5.406	0.000 00

(warming) and thus likely to have bigger shifts in lake ecology, relative to larger lakes. The lake temperature rates were larger than daily maximum or minimum air temperature, and there was no statistical difference in air temperatures across lake size at the 5% level of significance. Winslow et al. (2015) found small lakes in Wisconsin to be warming (0.42°C decade^{-1}) differently than large lakes, with muted change at deeper depths, potentially attributed to less wind from landscape positioning and therefore less turbulent mixing. We show that scale also played an important factor in ecosystem behavior with small lakes warming more rapidly. This has important considerations for ecosystem services given their role in fisheries, biodiversity, and providing an aquatic habitat deemed critical for many species that reside in this niche (Woodward et al. 2010). Further, these results emphasize potential risk to small lakes and ponds as often watersheds and land-use policy relies on networks of smaller ponds and wetlands to filter nutrients and regulate hydrological processes.

On average, the log-transformed elevation of the lake also has a significant negative effect on the lake temperature trends. Higher elevation ecotones have been proposed as acting as a surrogate for at risk environments, such as the Arctic. These results indicate that lakes in higher elevations in NNE, on average, were not increasing as quickly. It is possible these results were confounded with other factors, such as landscape heterogeneity or poorer data quality in mountainous regions. Collectively, these outcomes showed that local and landscape conditions influence lake temperature trends and not just regional air temperature alone in NNE. By using the results of the space–time model, decision-makers can better identify bodies of water that have greater risk of shifts in temperature or ecology to focus monitoring.

The space–time model evaluation was summarized in Table 3. The spatiotemporal and geodrivers explain much of the patterns in this region, but if these were included without the spatial dependence, only 47% of temperature variation in this region could be explained. The full model had moderate R^2, where 66% of temperature variation in this region was explained by the selected drivers.

Table 3. Summary of space–time model fit.

	R^2	RMSE
Mean field	0.4729	2.3132
Full model	0.6661	1.8412

This also suggests it was possible other factors, such as antecedent winter lake conditions, were an important driver of lake skin temperature in NNE over the past three decades.

A comparison of the maximum likelihood estimates of the spatially varying basis coefficients to the exploratory individual regression coefficients shows that in general the values were similar. Intercepts from both analyses can be interpreted as the average lake temperature from 1984 to 2014. The spatial patterns of the two methods' intercepts were similar but, in general, the spatially varying estimates were slightly cooler then the individual estimates. As noted, while a handful of regions in the northwest and far eastern Maine appear as "hot spots," the pattern was influenced by neighbor lakes not changing as rapidly, which was insignificant due to a lack of observations during key temporal windows. There were more differences between the trends estimated by the two analyses with the most differences in Maine lakes. Using both approaches helped provide more thorough understanding of lake temperature patterns (Figure 9).

5. Conclusions

Nearly 4000 lakes across northern New England were assessed for spatio-temporal trends in lake skin temperature. Results showed that most lakes in this region warmed with an average increase of 0.8°C decade^{-1} with smaller lakes warming more rapidly. The lake temperature trends warmed at a rate faster than air temperature trends on average. No major hot spots of change were found in NNE and high landscape heterogeneity in skin temp trends was present across the study region. Robust and complementing statistical approaches had similar outcomes and found maximum and minimum air temperature, lake size, and elevation to influence patterns. This work showed lake temperatures have on average increased and will continue to increase if projections remain accurate. To the best of our knowledge this presents the first comprehensive regional assessment of lake temperature trends. By using relatively automated techniques, the approach is potentially scalable and transferable to other regions. Data continuity from recently launched Landsat 8 operational land imager (OLI) and planned Landsat 9 in the near future will ensure continued capabilities to monitor lake skin temperature.

6. Future directions

Future work will focus on evaluating the transferability to additional regions, inclusion of imagery from other seasons, additional geodrivers, and complementing statistical analyses. For example, executing the analyses for all of the continental United States (CONUS) or North America would be a BigData computational challenge and provide valuable information. Winter ice cover and

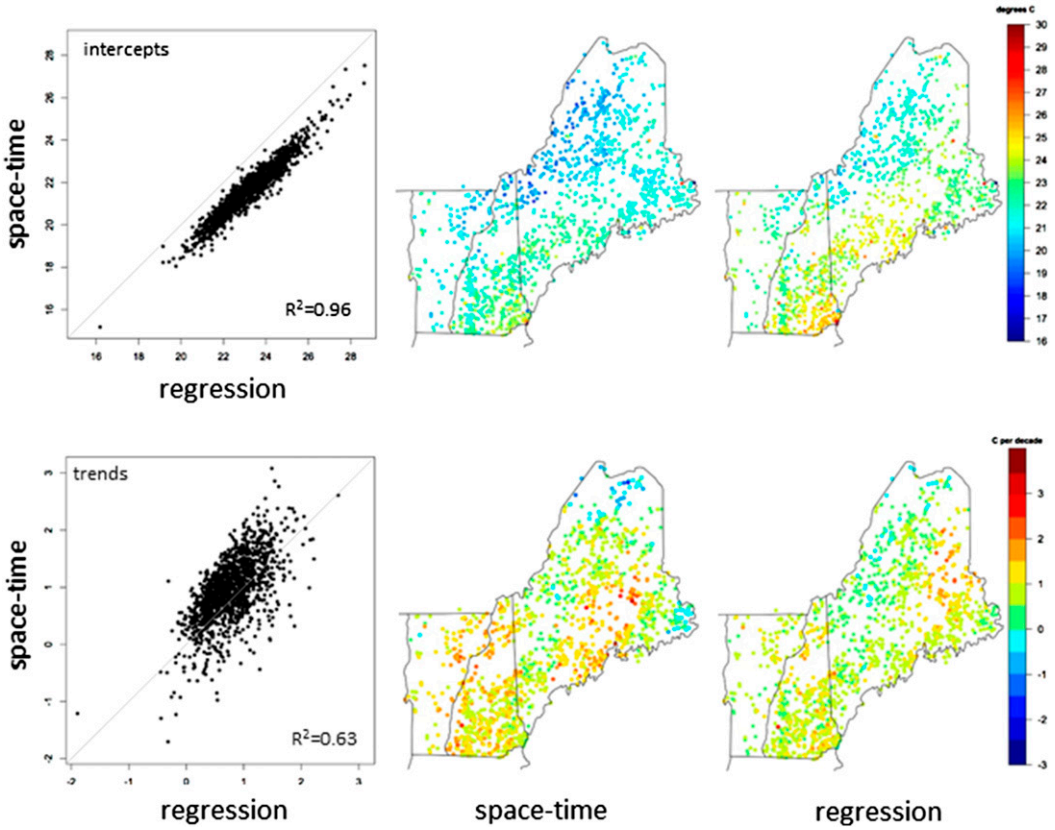

Figure 9. Spatially varying exploratory individual regression temperature and trend coefficients for mapping spatiotemporal lake skin temperature trends in NNE using Landsat. The regression approached tended to slightly underestimate intercept values, and these have strong agreement (R^2 = 0.96) and generally show warmer temperatures near the coast. Both techniques show similar spatial and temporal trends with moderate correlation (R^2 = 0.63) and illustrate highly variable local warming trends.

clouds were other variables of particular interest. Blending of fine, moderate, and coarse-scale imagery can provide more insight into variability and precision. A Bayesian approach of estimation would allow for more uncertainty quantification of the basis function coefficients. Alternatively, an approach could consider the use of a predictive process as described in Banerjee et al. (2008) and Finley (2011) or the use of Markov random fields and integrated nested Laplace approximations (INLA; Rue et al. 2009) to model the spatial–temporal structure. For these reason we suggest careful considerations should be used in characterizing the outcomes and drawing conclusions.

Acknowledgments. This work was supported in part by the National Institutes of Health (NIH) National Institute of Environmental Health Sciences (NIEHS) Grant R44 ES022103-03 and the National Science Foundation (NSF) Geography and Spatial Sciences (GSS)

Grant 1433756. Thanks to Bobby Braswell and Megan Corbiere for their help in processing Daymet and compiling Landsat data, respectively. We thank reviewers for their helpful comments.

References

Bailey, T., and A. Gatrell, 1995: *Interactive Spatial Data Analysis*. Wiley, 413 pp.

Banerjee, S., A. E. Gelfand, A. O. Finley, and H. Sang, 2008: Gaussian predictive process models for large spatial data sets. *J. Roy. Stat. Soc.*, **70B**, 825–848, doi:10.1111/j.1467-9868.2008.00663.x.

Cressie, N., and C. K. Wikle, 2011: *Statistics for Spatio-Temporal Data*. Wiley, 588 pp.

Finley, A. O., 2011: Comparing spatially-varying coefficients models for analysis of ecological data with non-stationary and anisotropic residual dependence. *Methods Ecol. Evol.*, **2**, 143–154, doi:10.1111/j.2041-210X.2010.00060.x.

Fu, F. X., Y. Zhang, M. E. Warner, Y. Feng, J. Sun, and D. A. Hutchins, 2008: A comparison of future increased CO_2 and temperature effects on sympatric *Heterosigma akashiwo* and *Prorocentrum minimum*. *Harmful Algae*, **7**, 76–90, doi:10.1016/j.hal.2007.05.006.

Hayhoe, K., and Coauthors, 2007: Past and future changes in climate and hydrological indicators in the US Northeast. *Climate Dyn.*, **28**, 381–407, doi:10.1007/s00382-006-0187-8.

——, and Coauthors, 2008: Regional climate change projections for the Northeast USA. *Mitigation Adapt. Strategies Global Change*, **13**, 425–436, doi:10.1007/s11027-007-9133-2.

Irish, R., J. Barker, S. Goward, and T. Arvidson, 2006: Characterization of the Landsat-7 ETM+ Automated Cloud-Cover Assessment (ACCA) algorithm. *Photogramm. Eng. Remote Sensing*, **72**, 1179–1188, doi:10.14358/PERS.72.10.1179.

Lenters, J., 2015: The Global Lake Temperature Collaboration (GLTC). *LakeLine Magazine*, Fall 2015, 9–12. [Available online at http://laketemperature.org/Documents/GLTC2015LL.pdf.]

——, S. J. Hook, and P. McIntyre, 2012: Workshop examines warming of lakes worldwide. *Eos, Trans. Amer. Geophys. Union*, **93**, 427, doi:10.1029/2012EO430004.

Lindström, J., A. Szpiro, P. D. Sampson, S. Bergen, and L. Sheppard, 2013: SpatioTemporal: An R package for spatio-temporal modelling of air-pollution. R package, 34 pp. [Available online at https://cran.r-project.org/web/packages/SpatioTemporal/vignettes/ST_intro.pdf.]

——, A. A. Szpiro, P. D. Sampson, A. P. Oron, M. Richards, T. V. Larson, and L. Sheppard, 2014: A flexible spatio-temporal model for air pollution with spatial and spatio-temporal covariates. *Environ. Ecol. Stat.*, **21**, 411–433, doi:10.1007/s10651-013-0261-4.

Masek, J. G., 2006: A Landsat surface reflectance dataset for North America, 1990-2000. *IEEE Geosci. Remote Sens. Lett.*, **3**, 68–72, doi:10.1109/LGRS.2005.857030.

Matheron, G., 1963: Principles of geostatistics. *Econ. Geol.*, **58**, 1246–1266, doi:10.2113/gsecongeo.58.8.1246.

Moore, S. K., V. L. Trainer, N. J. Mantua, M. S. Parker, E. A. Laws, L. C. Backer, and L. E. Fleming, 2008: Impacts of climate variability and future climate change on harmful algal blooms and human health. *Environ. Health*, **7**, S4, doi:10.1186/1476-069X-7-S2-S4.

——, N. J. Mantua, B. M. Hickey, and V. L. Trainer, 2009: Recent trends in paralytic shellfish toxins in Puget Sound, relationships to climate, and capacity for prediction of toxic events. *Harmful Algae*, **8**, 463–477, doi:10.1016/j.hal.2008.10.003.

Omernik, J. M., 1987: Ecoregion of the conterminous United States. *Ann. Assoc. Amer. Geogr.*, **77**, 118–125, doi:10.1111/j.1467-8306.1987.tb00149.x.

O'Reilly, C. M., and Coauthors, 2015: Rapid and highly variable warming of lake surface waters around the globe. *Geophys. Res. Lett.*, **42**, 10 773–10 781, doi:10.1002/2015GL066235.

Paerl, H. W., and J. Huisman, 2008: Blooms like it hot. *Science*, **320**, 57–58, doi:10.1126/science.1155398.

——, and ——, 2009: Climate change: A catalyst for global expansion of harmful cyanobacterial blooms. *Environ. Microbiol. Rep.*, **1**, 27–37, doi:10.1111/j.1758-2229.2008.00004.x.

——, and T. G. Otten, 2013: Harmful cyanobacterial blooms: Causes, consequences, and controls. *Microbiol. Ecol.*, **65**, 995–1010, doi:10.1007/s00248-012-0159-y.

——, N. Hall, and E. Calandrino, 2011: Controlling harmful cyanobacterial blooms in a world experiencing anthropogenic and climate-induced change. *Sci. Total Environ.*, **409**, 1739–1745, doi:10.1016/j.scitotenv.2011.02.001.

Peña, E. A., and E. H. Slate, 2006: Global validation of linear model assumptions. *J. Amer. Stat. Assoc.*, **101**, 341–354, doi:10.1198/016214505000000637.

Rue, H., S. Martino, and N. Chopin, 2009: Approximate Bayesian inference for latent Gaussian models by using integrated nested Laplace approximations (with discussion). *J. Roy. Stat. Soc.*, **71B**, 319–392, doi:10.1111/j.1467-9868.2008.00700.x.

Schneider, P., and S. J. Hook, 2010: Space observations of inland water bodies show rapid surface warming since 1985. *Geophys. Res. Lett.*, **37**, L22405, doi:10.1029/2010GL045059.

——, ——, R. K. Radocinski, G. K. Corlett, S. G. Hulley, S. G. Schladow, and T. E. Steissberg, 2009: Satellite observations indicate rapid warming trend for lakes in California and Nevada. *Geophys. Res. Lett.*, **36**, L22402, doi:10.1029/2009GL040846.

Schott, J. R., S. J. Hook, J. A. Barsi, B. L. Marham, J. Miller, F. P. Padula, and N. G. Raqueno, 2012: Thermal infrared radiometric calibration of the entire Landsat 4, 5, and 7 archive (1982–2010). *Remote Sens. Environ.*, **122**, 41–49, doi:10.1016/j.rse.2011.07.022.

Stumpf, R., T. Wynne, D. Baker, and G. Fahnenstiel, 2012: Interannual variability of cyanobacterial blooms in Lake Erie. *PLoS One*, **7**, e42444, doi:10.1371/journal.pone.0042444.

Torbick, N. M., and M. Corbiere, 2015: Mapping urban sprawl and impervious surfaces in the Northeast United States for the past four decades. *GIsci. Remote Sens.*, **52**, 746–764, doi:10.1080/15481603.2015.1076561.

——, S. Hession, S. Hagen, N. Wiangwang, B. Becker, and J. Qi, 2013: Mapping inland lake water quality across the lower peninsula of Michigan using Landsat TM imagery. *Int. J. Remote Sens.*, **34**, 7607–7624, doi:10.1080/01431161.2013.822602.

——, ——, E. Stommel, and T. Caller, 2014: Mapping amyotrophic lateral sclerosis lake risk factors across northern New England. *Int. J. Health Geographics*, **13**, 1–14, doi:10.1186/1476-072X-13-1.

Wake, C., E. Burekowski, P. Wilkinson, K. Hayhoe, A. Stoner, C. Keely, and J. LaBranche, 2014: Climate change in northern New Hampshire: Past, present and future. The Sustainability Institute Rep., 76 pp. [Available online at https://sustainableunh.unh.edu/sites/sustainableunh.unh.edu/files/images/northernnhclimateassessment2014.pdf.]

Weyhenmeyer, G. A., M. Meili, and D. Livingstone, 2004: Nonlinear temperature response of lake ice breakup. *Geophys. Res. Lett.*, **31**, L07203, doi:10.1029/2004GL019530.

Winslow, L., J. Read, G. Hansen, and P. Hanson, 2015: Small lakes show muted climate change signal in deepwater temperatures. *Geophys. Res. Lett.*, **42**, 355–361, doi:10.1002/2014GL062325.

Woodward, G., D. Perkins, and L. Brown, 2010: Climate change and freshwater ecosystems: Impacts across multiple levels of organization. *Philos. Trans. Roy. Soc. London*, **B365**, 2093–2106, doi:10.1098/rstb.2010.0055.

Zhang, G., T. Yao, H. Xie, J. Qin, Q. Ye, Y. Dai, and R. Guo, 2014: Estimating surface temperature changes of lakes in the Tibetan Plateau using MODIS LST data. *J. Geophys. Res. Atmos.*, **119**, 8552–8567, doi:10.1002/2014JD021615.

Zhong, Y., M. Notaro, S. Vavrus, and M. Foster, 2016: Recent accelerated warming of the Laurentian Great Lakes: Physical drivers. *Limnol. Oceanogr.*, **61**, 1762–1786, doi:10.1002/lno.10331.